



## Research article

# Comparison of left- and right-sided colorectal cancer to explore prognostic signatures related to pyroptosis

Shibi Luo<sup>a,1</sup>, Shenggang Cai<sup>a,1</sup>, Rong Zhao<sup>a</sup>, Lin Xu<sup>a</sup>, Xiaolong Zhang<sup>a</sup>, Xiaolei Gong<sup>a</sup>, Zhiping Zhang<sup>b,\*\*</sup>, Qiyu Liu<sup>a,\*</sup>

<sup>a</sup> Department of General Surgery, Ganmei Affiliated Hospital of Kunming Medical University (First People's Hospital of Kunming), Kunming, Yunnan, 650034, China

<sup>b</sup> Department of General Surgery, Affiliated Hospital of Yunnan University, Kunming, Yunnan, 650031, China

## ARTICLE INFO

## Keywords:

Left-sided colorectal cancer  
Right-sided colorectal cancer  
Pyroptosis  
Prognosis  
Predictive model  
Experimental validation

## ABSTRACT

**Background:** Colorectal cancer (CRC) is one of the most common malignancies, and pyroptosis exerts an immunoregulatory role in CRC. Although the location of the primary tumor is a prognostic factor for patients with CRC, the mechanisms of pyroptosis in left- and right-sided CRC remain unclear.

**Methods:** Expression and clinical data were collected from The Cancer Genome Atlas and Gene Expression Omnibus databases. Differences in clinical characteristics, immune cell infiltration, and somatic mutations between left- and right-sided CRC were then compared. After screening for differentially expressed genes, Pearson correlation analysis was performed to select pyroptosis-related genes, followed by a gene set enrichment analysis. Univariate and multivariate Cox regression analyses were used to construct and validate the prognostic model and nomogram for predicting prognosis. Collected left- and right-sided CRC samples were subjected to reverse transcription-quantitative polymerase chain reaction (RT-qPCR) to validate the expression of key pyroptosis-related genes.

**Results:** Left- and right-sided CRC exhibited significant differences in clinical features and immune cell infiltration. Five prognostic signatures were identified from among 134 pyroptosis-related differentially expressed genes to construct a risk score-based prognostic model, and adverse outcomes for high-risk patients were further verified using an external cohort. A nomogram was also generated based on three independent prognostic factors to predict survival probabilities, while calibration curves confirmed the consistency between the predicted and actual survival. Experiment data confirmed the significant differential expression of five genes between left- and right-sided CRC.

**Conclusion:** The five identified pyroptosis-related gene signatures may be potential biomarkers for predicting prognosis in left- and right-sided CRC and may help improve the clinical outcomes of patients with CRC.

\* Corresponding author. Department of General Surgery, Ganmei Affiliated Hospital of Kunming Medical University (First People's Hospital of Kunming), No. 504 Qingnian Road, Kunming, Yunnan, 650034, China.

\*\* Corresponding author. Department of General Surgery, Ganmei Affiliated Hospital of Kunming Medical University (First People's Hospital of Kunming), No. 504 Qingnian Road, Kunming, Yunnan, 650034, China.

E-mail addresses: [zhangzp0419@163.com](mailto:zhangzp0419@163.com) (Z. Zhang), [liuqiyu0415@163.com](mailto:liuqiyu0415@163.com) (Q. Liu).

<sup>1</sup> Shibi Luo and Shenggang Cai should be regarded as co-first authors.

## 1. Introduction

Colorectal cancer (CRC) is a common malignancy of the digestive system, with an extremely high incidence, accounting for 6% of the global cancer incidence in 2020 and ranking fifth among cancers in terms of morbidity and mortality [1,2]. Despite the series of approaches, including chemotherapy [3], immunotherapy [4,5], and targeted therapy [6], used in cancer treatment, less than 20% of patients with metastatic CRC survive more than 5 years [7].

CRC can be categorized into proximal right- or distal left-sided tumors based on the location of the primary tumor [8]. Right-sided CRC arises from the cecum, ascending colon, and hepatic flexion, whereas left-sided CRC originates from the splenic flexion, descending colon, and sigmoid colon [9]. Differences in embryonic origin and genetic, physiological, and clinical characteristics of different tumor sites may affect tumor behavior and pathological processes [10]. RNA sequencing and gene mutation analysis have suggested the presence of key molecular differences between left- and right-sided CRC that can accurately distinguish the location of tumor occurrence in patients with CRC [11]. Furthermore, the primary tumor side is considered a prognostic factor in patients with metastatic CRC [12] and may affect the prognosis of adjuvant therapy and overall survival (OS) of patients receiving palliative chemotherapy or targeted therapy [13,14]. Furthermore, a meta-analysis has indicated that tumor location is associated with survival and the prognosis of CRC [15]. However, specific biomarkers that can be used to predict the prognosis of left- and right-sided CRC remain limited.

Pyroptosis is a type of programmed cell death mediated by caspase-1 and may contribute to tumor progression [16]. It is activated by inflammasomes and causes cell swelling, plasma membrane lysis, and the release of intracellular pro-inflammatory cytokines [17]. These cytokines and immunogenic substances can promote immune cell activation and invasion, thereby leading to an inflammatory response and substantial tumor regression [18]. Therefore, pyroptosis is critical for the tumor immune microenvironment.

It is speculated that pyroptosis is closely related to CRC. Bioinformatics analysis identified 13 gene signatures related to pyroptosis and found that their expression levels were closely associated with OS, tumor purity, and immune checkpoints in patients with CRC [19]. Additionally, a risk model based on pyroptosis-related genes was constructed to assess and predict the prognosis of CRC patients [20]. Considering the potential mechanism of pyroptosis, the NLRs3, AIM24, and GSDM5 families may play important roles in pyroptosis signaling pathways in intestinal cancer [21]. Furthermore, GSDME-mediated pyroptosis was found to release HMGB1 and induce tumor cell proliferation through the ERK1/2 pathway, thereby promoting CRC progression [22]. Additionally, pyroptosis in CRC is reportedly regulated by several microRNAs, such as miR-21-5p and miR-448 [23,24]. However, the effect of pyroptosis on the prognosis of CRC at different tumor locations and the underlying molecular mechanisms remain unknown.

In the current study, bioinformatics methods were used to compare differences in clinical characteristics, immune infiltration, gene mutations, and gene expression levels between patients with left- and right-sided CRC based on The Cancer Genome Atlas (TCGA) and Gene Expression Omnibus (GEO) databases. From among differentially expressed genes (DEGs), pyroptosis-related gene signatures with prognostic independence were screened, and prognostic and nomogram models were constructed to predict the prognosis of CRC. This study proposed and validated molecular alterations among patients with CRC at different tumor locations and explored the risk factors influencing their prognoses based on the mechanism of cell pyroptosis.

## 2. Methods

### 2.1. Data collection and pre-processing

Gene expression RNA sequencing of the pan-cancer Genomic Data Commons, and phenotypes of colon and rectal cancer were downloaded from TCGA database [25]. Among them, the ascending colon, transverse colon, and cecum were classified as the right-sided colon, and the descending colon, sigmoid colon, and rectum were categorized as the left-sided colon. A total of 271 left-sided and 221 right-sided CRC samples with information on OS were obtained. Based on the annotation file of the platform, Ensembl\_ID was converted to Symbol\_ID in the Gencode database [26] to get access to the mRNA expression matrix. The GSE72970 dataset, comprising 88 left- and 36 right-sided CRC samples with OS information, was downloaded from the GEO database and used as an external validation cohort.

### 2.2. Comparison of clinicopathologic features

To compare the differences in clinical manifestations between left- and right-sided CRC, we collected clinical phenotypes (including age, sex, tumor node metastasis stage, and pathologic stage) of each sample and analyzed the sample distribution of the two groups under different clinical characteristics using the R.ggstatsplot package (version 0.5.0) [27]. Statistical  $p$  was calculated using the chi-square test, and clinical factors with  $p$  values  $< 0.05$  were considered to be related to CRC tumor location. OS was also compared between the two groups using a Kaplan–Meier curve, which was created using the R.survival package (version 2.42–6) [28].

### 2.3. Immune infiltration analysis

CIBERSORT [29] was used to analyze the infiltration abundance of 22 types of immune cells in each tumor sample. Differences in immune infiltration between left- and right-sided CRC were then compared.

**Table 1**  
Primer sequences of five prognostic signatures detected in qRT-PCR.

Primer	Sequence (5' to 3')
TDGF1-F	TTTGAAGCTGGGATTAGTTGCCG
TDGF1-R	GGGGCCAAATGCTGTCATCT
TP63-F	GGACCAGCAGATTCAGAACGG
TP63-R	AGGACACGTCGAAACTGTGC
CHMP7-F	AAGCCTCTCAAGTGGACTCTT
CHMP7-R	ACAGACGATACACCTCCTCAG
NLRP7-F	CGAAGACGTGCTACAGAAGAC
NLRP7-R	TTCACAGTCGCATTCTTATCC
CXCL13-F	GCTTGAGGTGTAGATGTGTCC
CXCL13-R	CCCACGGGGCAAGATTTGAA
GAPDH-F	TGCAACCGGGAAGGAAATGA
GAPDH-R	GCATCACCCGGAGGAGAAAT

qRT-PCR, quantitative real-time polymerase chain reaction; F, forward; R, reverse.

#### 2.4. Tumor mutation analysis

Using the Mutect software, the somatic mutation file of CRC was obtained from TCGA. R.Maftools (version 2.0.16) [30] was used to create a summary plot and to analyze the somatic mutant status of left- and right-sided CRC samples.

#### 2.5. Screening of DEGs related to pyroptosis between left- and right-sided CRC

The R.limma package (version 3.10.3) [31] was used to compare differences in mRNA expression between left- and right-sided CRC. Statistical significance was calculated using the *t*-test, and DEGs were selected at thresholds of  $p < 0.05$  and  $|\log\text{fold change (FC)}| > 1$ . DEGs between left- and right-sided CRC were visualized by volcano plots using the R.ggplot2 package (version 3.3.6) [32].

To further screen pyroptosis-related DEGs, we first collected pyroptosis-related genes from published articles [33,34] and obtained expression matrices of 48 pyroptosis-related genes after matching with TCGA dataset. The Pearson correlation coefficients of DEGs and 48 pyroptosis-related genes were calculated using the *cor.test* function in R [35]. Finally, pyroptosis-related DEGs with  $p < 0.05$  and  $|r| > 0.4$  were selected.

#### 2.6. Gene set enrichment analysis (GSEA)

Pyroptosis-related DEGs sorted by logFC were subjected to GSEA. This step was performed using the R.clusterProfiler package (version 3.16.0) [36] with *c2.cp.kegg.v7.4.symbols.gmt* in the MSigDB database [37] functioning as the enrichment background. Kyoto Encyclopedia of Genes and Genomes (KEGG) pathways with  $p < 0.05$  adjusted by the Benjamini-Hochberg method were considered statistically significant.

#### 2.7. Identification of prognostic signatures to construct and validate the risk score-based model

The univariate Cox regression analysis using the R package “survival” (version:2.42–6) was used to screen for pyroptosis-related DEGs that were significantly associated with OS [28]. Independent prognostic signatures were identified among the prognostic pyroptosis-related DEGs using multivariate Cox regression analysis. A *p*-value  $< 0.05$  was deemed statistically significant. According to the regression coefficients of the prognostic signatures and their expression levels, a risk score-based prognostic model was established as follows:

$$\text{Risk score} = \sum \text{Coef}_{\text{gene}} \times \text{Exp}_{\text{gene}}$$

where Coef indicates the prognostic coefficient of the multivariate Cox regression analysis, and  $\text{Exp}_{\text{gene}}$  indicates the expression levels of candidate genes in TCGA database [38]. Samples were grouped into high- and low-risk groups, and Kaplan–Meier curves were plotted to evaluate the association between risk scores and OS. The performance of the prognostic model was further validated based on the expression levels of candidate genes in GSE72970. Furthermore, we grouped samples according to the optimal value of candidate gene expression and assessed the relationship between gene expression and prognosis using the log-rank test and Kaplan–Meier analysis [39].

#### 2.8. Screening of independent prognostic factors to create a nomogram

Based on multiple clinical features, including age, sex, pathological stage, tumor stage, and risk score, independent prognostic factors were identified using univariate and multivariate Cox regression analyses. A *p*-value  $< 0.05$  was deemed statistically significant. A nomogram was generated using the nomogram function of R.rms (version 6.1–0) [40] to predict the 1-, 2-, and 3-year survival

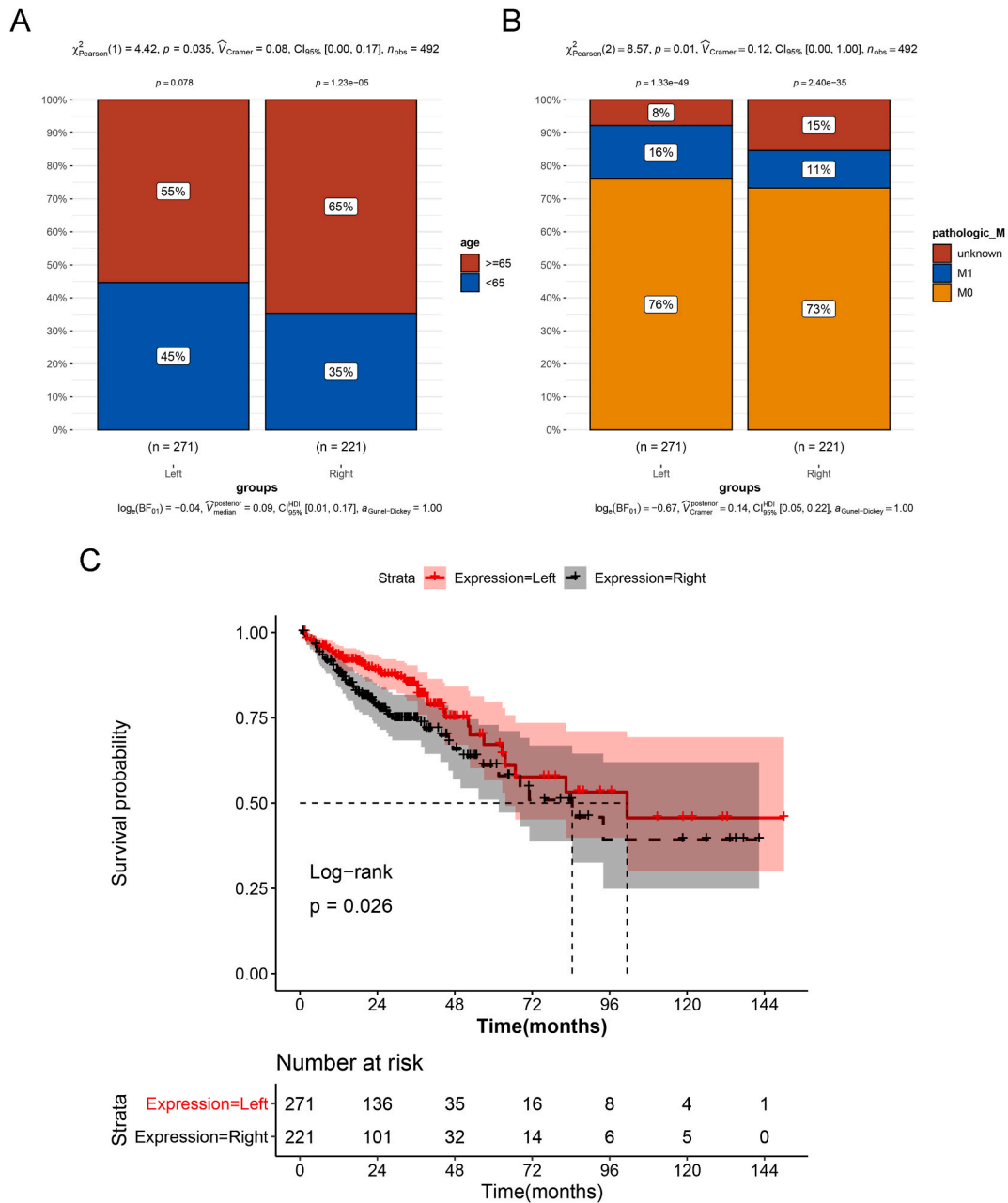


**Fig. 1. Differences in clinical features between left- and right-sided colorectal cancer.** A–B: The distributions of age (A) and pathological metastasis stage (B) differs significantly among patients with CRC at different tumor locations. C: The Kaplan–Meier curve illustrates the survival difference between the two groups. CRC, colorectal cancer.

probabilities, followed by generation of calibration curves to evaluate the predictive power of the nomogram.

### 2.9. Enrichment analysis of DEGs between high- and low-risk samples

Gene expression between the high- and low-risk groups was performed using the *t*-test from the R.limma package. The clusterProfiler [36] package was employed to perform KEGG pathway [41] and Gene Ontology biological processes (GO-BPs) [42] analyses of DEGs between the high- and low-risk groups. Terms with an enriched gene count  $\geq 2$  and  $p < 0.05$  were regarded as statistically significant.

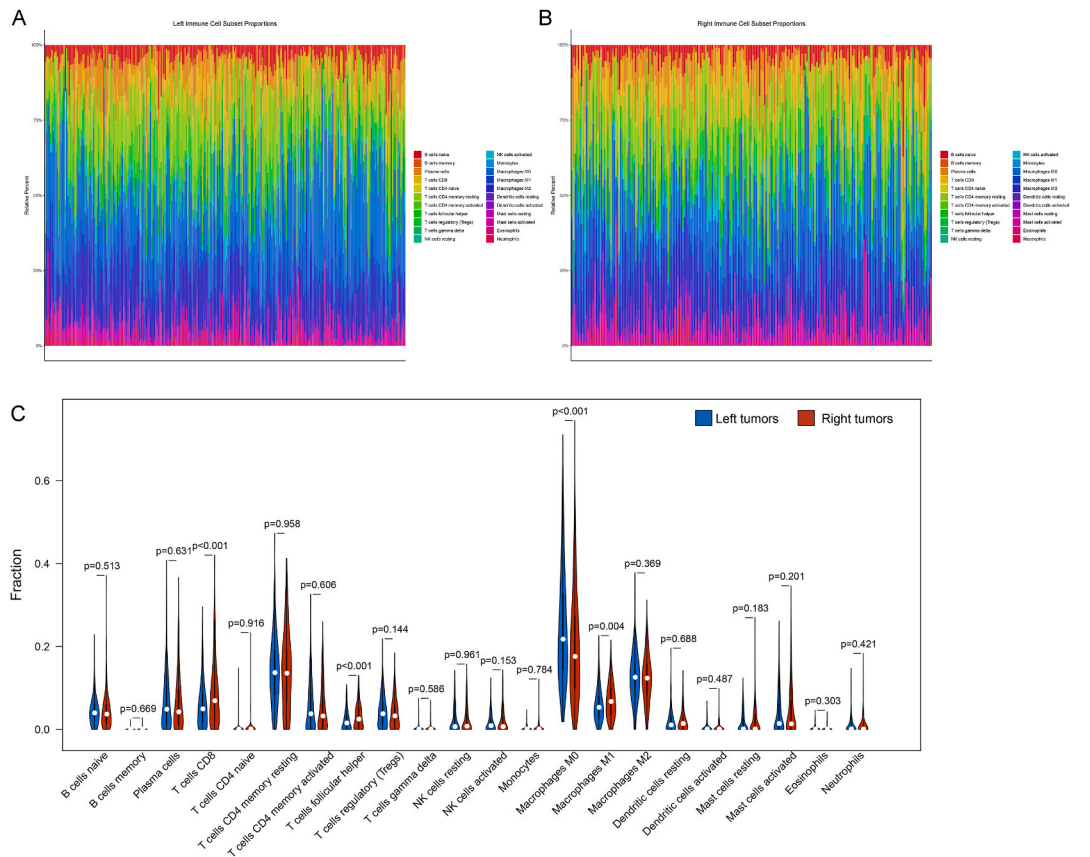


**Fig. 2.** Analysis of immune infiltration among left- and right-sided colorectal cancer. A–B: Infiltration fractions of 22 types of immune cells in all left- (A) and right-sided (B) CRC samples. C: Immune infiltration was compared between left- and right-sided CRC, and statistical significance was set at  $p < 0.05$ . CRC, colorectal cancer.

### 2.10. Clinical sample collection

A total of 10 patients pathologically diagnosed with CRC at the First People's Hospital of Kunming were enrolled in this study. Among them, five cases with primary tumors located in the ascending colon, transverse colon, and cecum were assigned to the right-sided CRC group, while five cases with primary tumors located in the descending colon, sigmoid colon, and rectum were included in the left-sided CRC group. Clinical information pertaining to these 10 patients was organized in [Supplementary Table 1](#). All patients had no autoimmune disease or previous history of cancer and had not received chemotherapy, radiotherapy, or other antitumor drugs prior to tumor resection. The study complied with the declaration of Helsinki and was approved by the ethics committee of First People's Hospital of Kunming (YLS2023-97). All subjects signed informed consent forms.

### 2.11. Reverse transcription-quantitative polymerase chain reaction (RT-qPCR)

All samples were ground and then added to Trizol (9109, TaKaRa) for RNA extraction. After evaluating RNA concentration and quality, the samples were subjected to reverse transcription reaction and PCR amplification. Finally, mRNA expression levels of key pyroptosis-related genes were assessed using a PCR machine (7900HT FAST, ABI). For the accuracy of the results, at least three replicates were performed for each group. Detailed primer sequences are displayed in [Table 1](#). The data was analyzed using the  $2^{-\Delta\Delta Ct}$  algorithm by normalizing expression levels to glyceraldehyde 3-phosphate dehydrogenase (GAPDH) expression.

### 2.12. Statistical analysis

Statistical analyses and plotting of graphs were performed using GraphPad Prism 9.0.5 (GraphPad Software, Inc., San Diego, CA). Comparisons between two groups were performed using the unpaired  $t$ -test, and all results are presented as the mean  $\pm$  standard deviation. The statistical significance was set at  $p < 0.05$ .

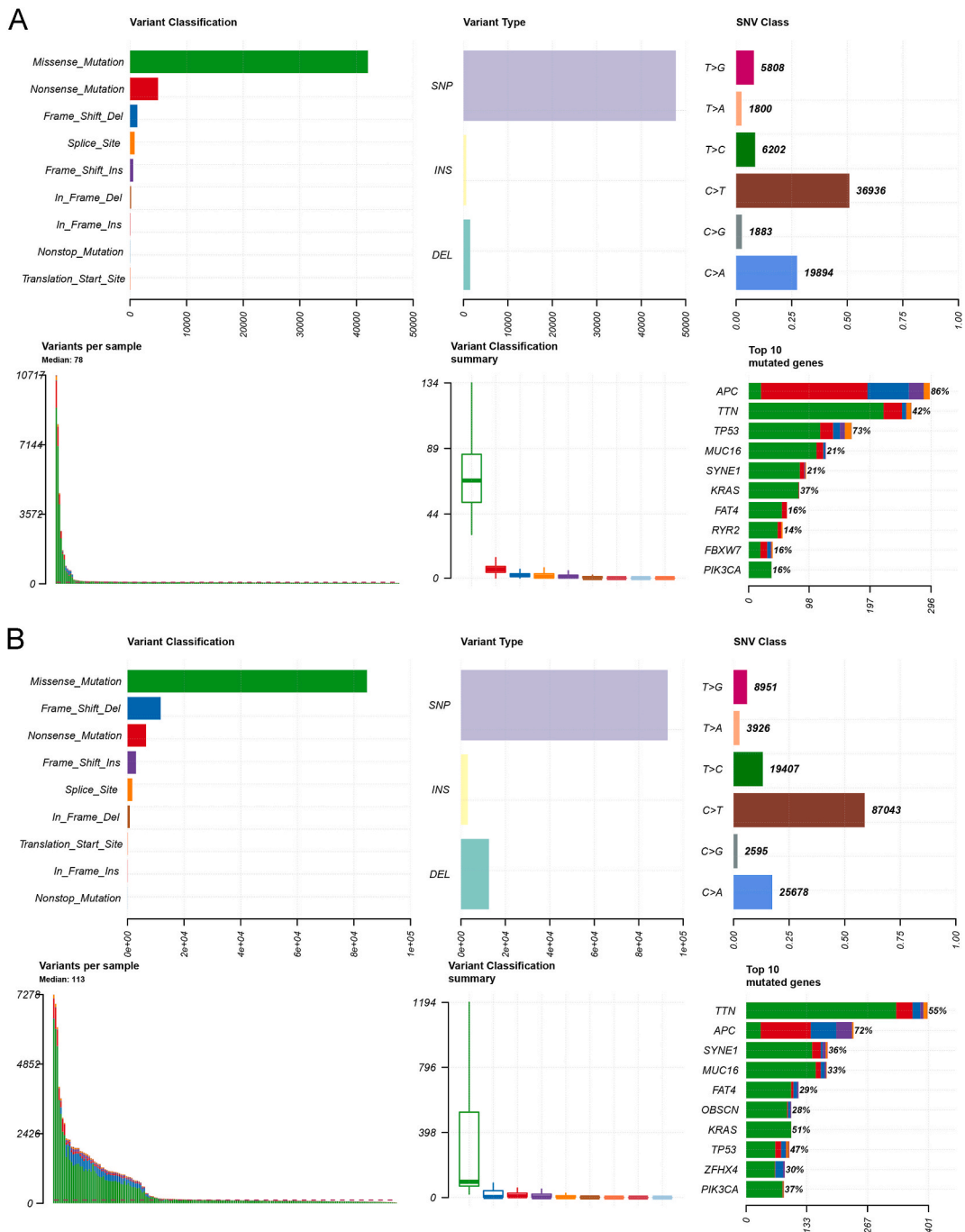


**Fig. 3.** The somatic mutation status of left- (A) and right-sided (B) colorectal cancer samples summarized in terms of variant classification, variant type, and mutation frequency.

### 3. Results

#### 3.1. Comparison of clinical characteristics between left- and right-sided CRC

Differences in clinical characteristics between 271 left-sided CRC samples and 221 right-sided CRC samples were analyzed in this study, as shown in [Supplementary Table 2](#). Age, pathological metastasis stage, and survival status differed significantly between the two groups. To verify the results, we also compared the distribution of samples with distinct clinical characteristics between the two groups. We found that there were significant between-group differences in the distribution of patients in terms of age and metastasis

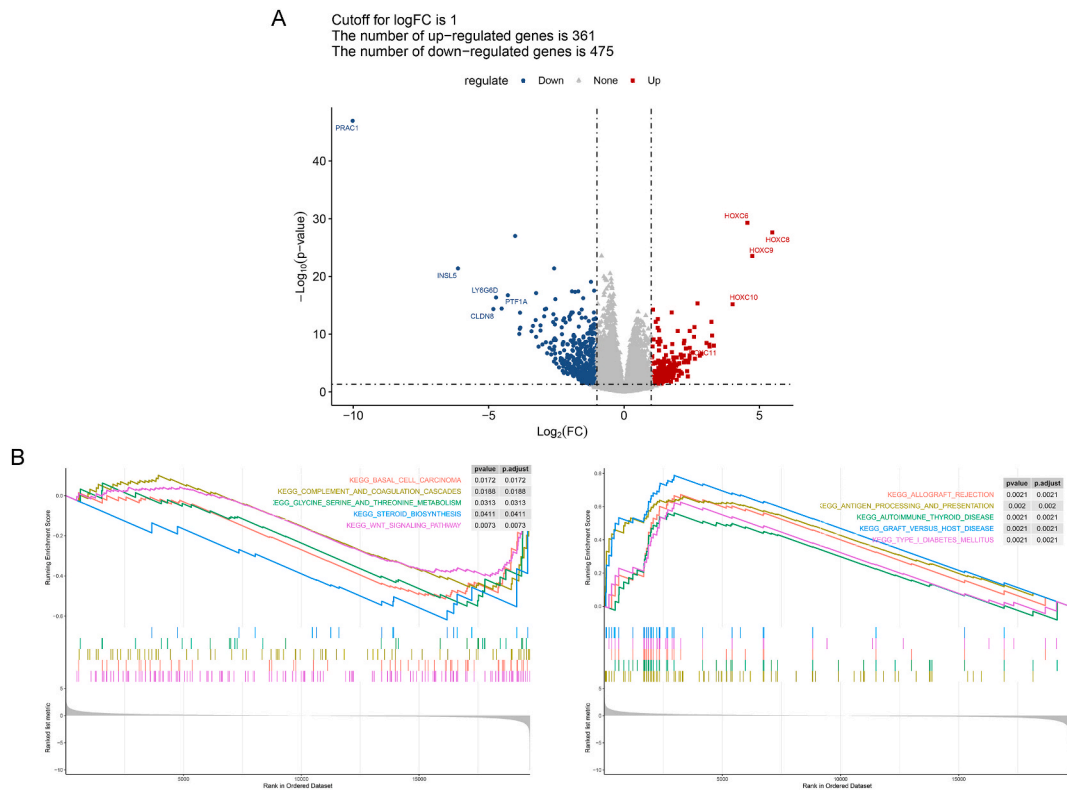


**Fig. 4. Identification of pyroptosis-related genes between left- and right-sided colorectal cancer and gene set enrichment analysis.** A: Volcano plot showing 361 upregulated and 475 downregulated DEGs in the right-sided CRC compared with the left-sided CRC at the threshold of  $p < 0.05$  and  $|\log_{2}FC| > 1$ . B: Top five pathways with NES  $> 0$  (left) and top five pathways with NES  $< 0$  (right) in GSEA based on 134 pyroptosis-related DEGs. CRC, colorectal cancer; DEGs, differentially expressed genes; NES, normalized enrichment score; GSEA, gene set enrichment analysis.

stage (Fig. 1A and B). The survival difference was visualized using a Kaplan–Meier curve, and the results suggested that patients with right-sided CRC had an adverse prognosis when compared with those with left-sided CRC ( $p = 0.026$ , Fig. 1C).

### 3.2. Immune infiltration difference between left- and right-sided CRC

As described in the Methods section, we calculated the infiltration abundance of 22 types of immune cells for all left- (Fig. 2A) and right-sided (Fig. 2B) CRC samples. Differences in immune infiltration were then compared and illustrated using a violin plot (Fig. 2C). Four types of immune cells differed significantly in infiltration abundances. The infiltration of CD8 T cells, T follicular helper cells, and M1 macrophages was remarkably higher in patients with right-sided CRC than in those with left-sided CRC; however, patients with left-sided CRC exhibited significantly increased M0 macrophage infiltration.

### 3.3. Analysis of mutation status of left- and right-sided CRC

The somatic mutation status of left- and right-sided CRC was also analyzed and is shown as summary plots. Missense mutations were identified as the main classification of variants in both left- and right-sided CRC samples. Furthermore, the top 10 mutated genes in left-sided CRC were *APC*, *TTN*, *TP53*, *MUC16*, *SYNE1*, *KRAS*, *FAT4*, *RYR2*, *FBXW7*, and *PIK3CA* (Fig. 3A). Considering right-sided CRC, the top 10 genes with the highest mutation frequencies were *TTN*, *APC*, *SYNE1*, *MUC16*, *FAT4*, *OBSCN*, *KRAS*, *TP53*, *ZFH4*, and *PIK3CA* (Fig. 3B).

### 3.4. Screening of pyroptosis-related genes and GSEA

Based on the processed data, we compared mRNA expression levels between left- and right-sided CRC, identifying 836 DEGs (including 361 upregulated and 475 downregulated DEGs), as shown in Fig. 4A. We then estimated the relationships between 836 DEGs and 50 pyroptosis-related genes collected from published papers, finally obtaining 134 pyroptosis-related DEGs with thresholds of  $p < 0.05$  and  $|r| > 0.4$ .

After ranking the gene set according to logFC, GSEA was performed with KEGG pathways as the background. A total of 26 KEGG pathways were obtained (Table 2), of which six pathways were negatively correlated (normalized enrichment score [NES]  $> 0$ ), and 20

**Table 2**  
GSEA of pyroptosis-related DEGs between left- and right-sided CRC.

KEGG pathways	Enrichment Score	NES	adjust p
KEGG_ANTIGEN_PROCESSING_AND_PRESENTATION	0.661179208	2.266199478	0.00203666
KEGG_AUTOIMMUNE_THYROID_DISEASE	0.561785796	1.773646458	0.002057613
KEGG_ALLOGRAFT_REJECTION	0.673029598	1.977277154	0.002066116
KEGG_TYPE_1_DIABETES_MELLITUS	0.626924973	1.900427653	0.002079002
KEGG_GRAFT_VERSUS_HOST_DISEASE	0.788442015	2.338560295	0.002083333
KEGG_SYSTEMIC_LUPUS_ERYTHEMATOSUS	0.576379881	1.833604484	0.002087683
KEGG_HEMATOPOIETIC_CELL_LINEAGE	0.508706798	1.747633752	0.002114165
KEGG_INTESTINAL_IMMUNE_NETWORK_FOR_IGA_PRODUCTION	0.740390085	2.282364097	0.002114165
KEGG_LEISHMANIA_INFECTION	0.57575029	1.908415615	0.002132196
KEGG_NATURAL_KILLER_CELL_MEDIATED_CYTOTOXICITY	0.574450536	2.089643678	0.002188184
KEGG_CYTOKINE_CYTOKINE_RECEPTOR_INTERACTION	0.420342428	1.663437574	0.002336449
KEGG_ASTHMA	0.651036339	1.78879836	0.004166667
KEGG_WNT_SIGNALING_PATHWAY	-0.402171014	-1.436822935	0.007285974
KEGG_TOLL_LIKE_RECEPTOR_SIGNALING_PATHWAY	0.42453241	1.481282957	0.008888889
KEGG_BASAL_CELL_CARCINOMA	-0.514589951	-1.594710126	0.017175573
KEGG_COMPLEMENT_AND_COAGULATION_CASCADES	-0.468181315	-1.509505877	0.018761726
KEGG_T_CELL_RECEPTOR_SIGNALING_PATHWAY	0.408955279	1.448361504	0.019522777
KEGG_VIRAL_MYOCARDITIS	0.441439242	1.460864752	0.027659574
KEGG_JAK_STAT_SIGNALING_PATHWAY	0.360607959	1.341985658	0.028953229
KEGG_GLYCINE_SERINE_AND_THREONINE_METABOLISM	-0.550299301	-1.515341327	0.031311155
KEGG_ASCORBATE_AND_ALDARATE_METABOLISM	0.576262606	1.560865858	0.032653061
KEGG_STEROID_BIOSYNTHESIS	-0.618751558	-1.507694503	0.04109589
KEGG_PRIMARY_IMMUNODEFICIENCY	0.522016959	1.533620823	0.041322314
KEGG_DRUG_METABOLISM_CYTOCHROME_P450	0.411747929	1.373510758	0.042283298
KEGG_CHEMOKINE_SIGNALING_PATHWAY	0.336459724	1.27353271	0.043478261
KEGG_NEUROACTIVE_LIGAND_RECEPTOR_INTERACTION	-0.330605032	-1.271689665	0.045936396

GSEA: gene set enrichment analysis; DEG: differentially expressed genes; CRC: colorectal cancer; KEGG: Kyoto Encyclopedia of Genes and Genomes; NES: normalized enrichment score.

Statistical *p* value was adjusted by Benjamini-Hochberg method.

pathways had positive correlations ( $NES < 0$ ). The top five pathways with  $NES > 0$  and those with  $NES < 0$  are shown in Fig. 4B. We observed that the gene sets involved in allograft rejection, antigen processing and presentation, and autoimmune thyroid disease were mainly enriched in right-sided CRC. KEGG pathways with  $NES < 0$ , such as basal cell carcinoma and complement and coagulation cascades, were primarily enriched in left-sided CRC.

### 3.5. Screening of prognostic signatures to generate a prognostic model

Based on the 134 pyroptosis-related DEGs obtained, we further screened eight prognostic genes that were significantly correlated with OS using univariate Cox regression analysis (Fig. 5A). We then performed a multivariate Cox regression analysis and identified five prognostic signatures, including *CHMP7*, *CXCL13*, *NLRP7*, *TDGF1*, and *TP63* (Fig. 5B). Risk score-based prognostic models of the training and validation sets were constructed based on their expression levels and prognostic coefficients. The risk score of each sample was calculated to sort samples into two risk groups, followed by a comparison of OS between the two groups. The results suggested that patients with high-risk scores had substantially more adverse prognoses than those with low-risk scores in both the training and validation sets (Fig. 5C and D, respectively). We also plotted Kaplan-Meier curves to evaluate the associations between candidate gene expression and survival status and found that patients with high expression of *CHMP7*, *CXCL13*, *NLRP7*, and *TDGF1* had a significantly favorable prognosis, whereas increased *TP63* expression correlated with an adverse prognosis (Fig. 5E).

### 3.6. Construction of the nomogram model based on independent prognostic factors

To screen for independent prognostic factors from several clinical features, we performed univariate and multivariate Cox regression analyses (Fig. 6A and B). Age, pathological tumor stage, and risk score were identified as independent prognostic factors. Next, a nomogram model was constructed based on these independent prognostic factors to predict the 1-, 2-, and 3-year survival probabilities of patients (Fig. 6C). Calibration curves were created to verify the effectiveness of the nomogram in predicting survival status. The results indicated that the survival rates predicted by the model were consistent with the actual rates (Fig. 6D), suggesting the nomogram model had a satisfactory predictive performance.

### 3.7. Enrichment analysis of DEGs between the high- and low-risk prognostic groups

Differences in gene expression between the high-risk and low-risk groups were further compared, and we found 172 differentially expressed mRNAs, including 87 upregulated and 85 downregulated mRNAs. Enrichment analysis of functions and pathways of these genes was performed. Based on the results, upregulated mRNAs were mainly enriched in KEGG pathways of neuroactive ligand-

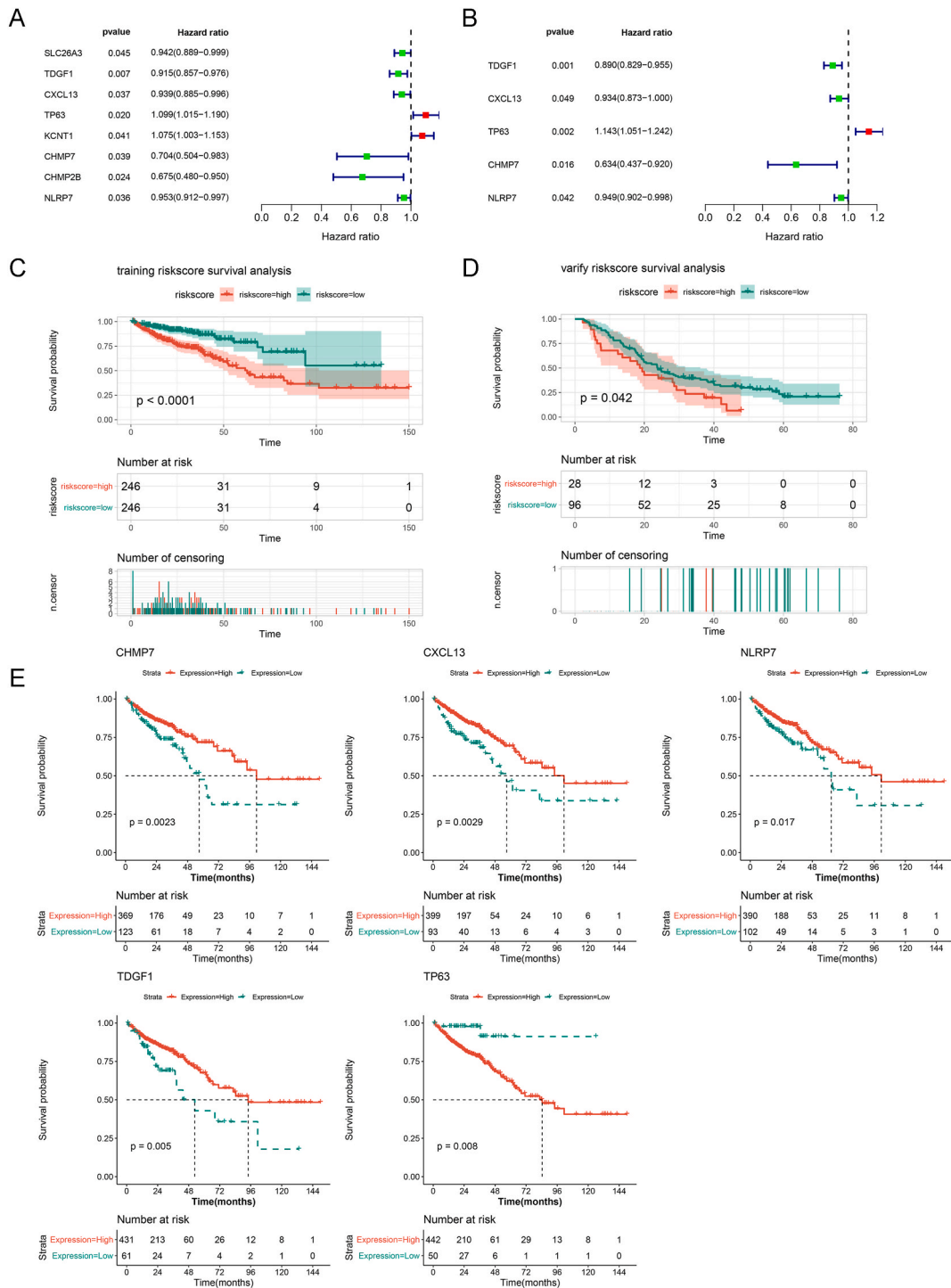


**Fig. 5. Identification of five prognostic signatures to construct and validate the risk score-based prognostic model.** A: Univariate Cox regression analysis was used to screen eight prognostic genes from 134 pyroptosis-related DEGs that correlated significantly with OS. B: Multivariate Cox regression analysis was used to further screen the five prognostic signatures. C–D: The risk score-based model was constructed using TCGA dataset and verified using the GSE72970 dataset. Kaplan–Meier curves show the survival differences between the high- and low-risk groups in both the training set (C) and validation set (D). E: Kaplan–Meier curves showing the relationship between the expression levels of candidate genes and OS status. OS, overall survival; DEGs, differentially expressed genes; TCGA, The Cancer Genome Atlas.

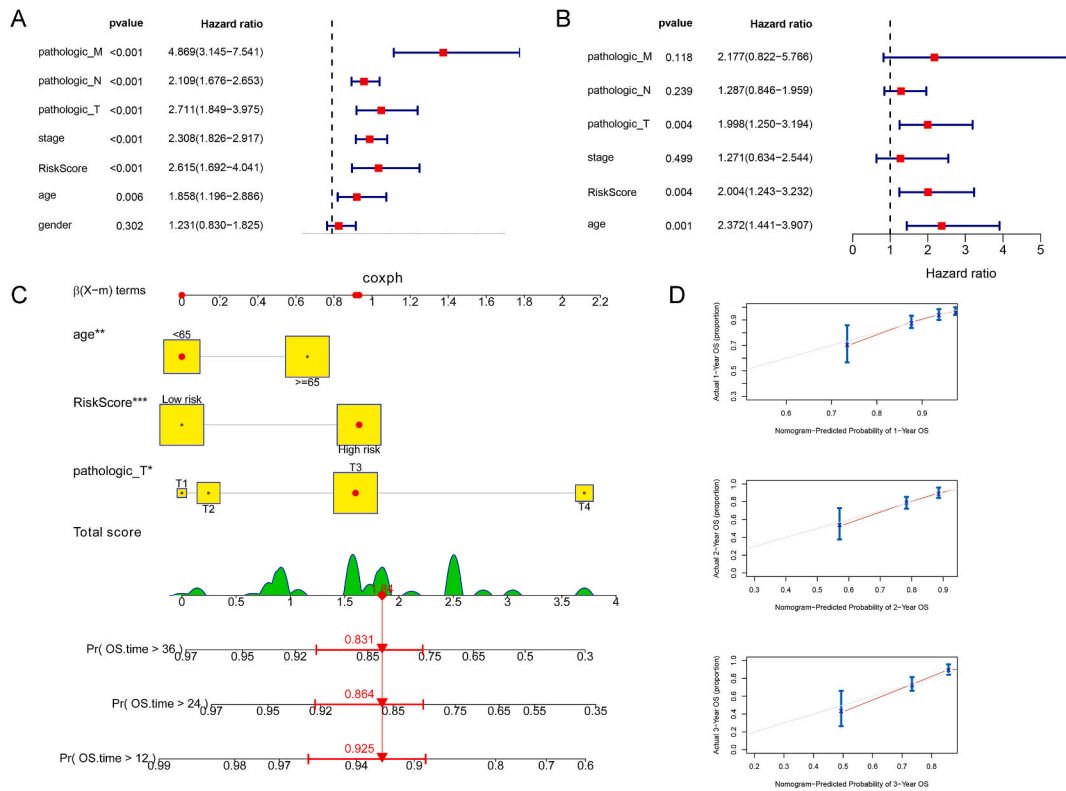


**Fig. 6.** Screening of independent prognostic factors and construction of a nomogram model to predict survival probabilities. A–B: Univariate (A) and multivariate (B) Cox regression analyses were performed to identify the independent risk factors associated with prognosis. C: A nomogram model was constructed based on these independent prognostic factors to predict the 1-, 2-, and 3-year survival probabilities of patients. D: Calibration curves were created to verify the effectiveness of the nomogram model in predicting survival status.

receptor interaction and cell adhesion (Fig. 7A) and GO-BPs of skin development and epidermis development (Fig. 7B); downregulated mRNAs were mainly involved in the cytokine-cytokine receptor interaction pathway (Fig. 7C) and GO-BPs of the humoral immune response, and B-cell activation (Fig. 7D).

### 3.8. Experiment validation of five prognostic signatures

Clinical tumor samples were collected for RT-qPCR to further explore the expression patterns of five prognostic signatures in CRC. Raw data of qRT-PCR are shown in Supplementary Table 3. Compared with left-sided CRC, right-sided CRC exhibited significantly increased expression of *TP63* expression (Fig. 8A), accompanied by significant under-expression of *TDGF1*, *CHMP7*, *NLRP7*, and *CXCL13* (Fig. 8B–E). These conclusions are consistent with the above findings and revealed that *TP63* may be a prognostic risk factor for CRC, while the remaining four genes may play prognostic protective roles.

## 4. Discussion

Upon comparing the clinical manifestations of left- and right-sided CRC based on expression data and clinical information available in public database sources, we revealed that right-sided CRC was associated with a higher prognostic risk and a greater proportion of aged patients than left-sided CRC. This phenomenon could be attributed to potential differences in immune cell infiltration and somatic mutations. To further identify the underlying molecular regulatory mechanisms of pyroptosis and their impact on prognosis, pyroptosis-related DEGs were screened between left- and right-sided CRC and five gene signatures with prognostic value were identified. Both prognostic models and nomograms based on these genes could predict the prognosis of CRC. Moreover, experimental data confirmed the differential expressions of these five genes between left- and right-sided CRC. Therefore, these five gene signatures may serve as potential markers for clarifying the prognosis of left- and right-sided CRC, and their involvement in the mechanism of pyroptosis may be key to the clinical outcomes of patients. The findings of the current study provide new insights into potential mechanisms underlying the prognostic differences between left- and right-sided CRC and may contribute to predicting the prognostic risk of CRC in patients with different tumor locations.

CRC is a heterogeneous disease with complex genetic features, and its primary tumor location may be associated with prognosis. Tumors arising in different locations in CRC are clinically and molecularly distinct and thus have been frequently regarded as diverse

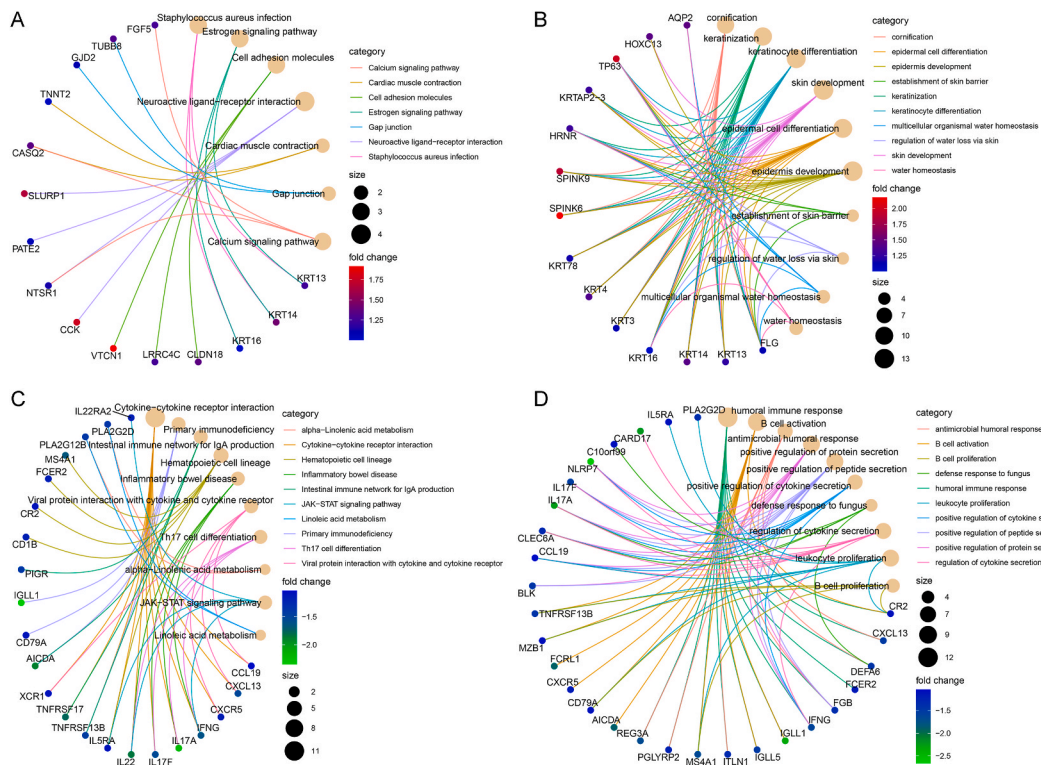


**Fig. 7.** Enrichment analysis of potential functions and pathways of differentially expressed mRNAs between the high- and low-risk groups. A–B: Top 10 enriched KEGG pathways (A) and GO-BPs (B) in 87 upregulated mRNAs. C–D: Top 10 enriched KEGG pathways (C) and GO-BPs (D) in 85 downregulated mRNAs. GO-BP, gene ontology biological processes; KEGG, Kyoto Encyclopedia of Genes and Genomes.

tumor entities [43]. By comparing the clinical features, we identified a significantly adverse clinical outcome in patients with right-sided CRC, which is consistent with the findings of most studies. Right-sided CRC has been associated with poor OS [44]. Moreover, in patients with stage III CRC, the OS rate of right colon tumors was worse than that of the left side [45].

However, some inconsistent conclusions have been raised and suggested that the laterality of the tumor does not significantly impact the overall prognosis of patients with CRC [46]. In this context, tumor stage may underlie the differences in the prognosis of CRC with different primary tumor locations. Reportedly, right-sided CRC has a lower mortality rate at stage II, whereas stage III right-sided CRC has a higher mortality rate than left-sided CRC [47]. Lymph node resection also affects the prognosis of tumors at different locations [48]. In addition to tumor stage and lymph node resection, age and sex may be potential prognostic factors. Related studies have suggested that right-sided CRC is more common in older patients and women and has a poor prognosis [49,50]. Our study also confirmed that right-sided CRC is more prevalent in patients aged > 65 years. Although these studies have suggested a substantial association between tumor location and prognosis in CRC, the direction of this association in terms of causality has not been clarified.

Changes in the immune microenvironment may also contribute indirectly to the difference in prognosis. Herein, we observed significant alterations in the levels of macrophage and T-cell infiltration between left- and right-sided CRC. Pyroptosis-related regulatory factors play crucial roles in the immune microenvironment and tumor development. Pyroptosis contributes to the activation of multiple cytokines and risk-related signaling molecules and is associated with immune infiltration and inflammatory responses [51]. Microparticles released by pyroptosis have been found to divert inflammatory mediators, regulate interactions between various cells, and lead to endothelial cell damage and macrophage infiltration [52]. Inflammasome-mediated pyroptosis also occurs in intestinal epithelial cells, and the cross-presentation of intestinal epithelial-derived antigens with CD8<sup>+</sup> T cells also depends on this process [53]. Therefore, we speculated that macrophages and CD8<sup>+</sup> T cells are interdependent with pyroptosis and may contribute to tumor induction and development. Interestingly, we also detected higher infiltration levels of macrophages with M0 and M2 phenotypes in left-sided CRC, with elevated M1 macrophage infiltration observed in right-sided CRC. These findings suggest that macrophage polarization exhibits distinct patterns in the immune microenvironment of left- and right-sided CRC and may affect the prognosis of CRC. Our findings align with those of relevant studies and suggest that macrophage polarization status is associated with CRC survival, while M1 and M2 phenotypes play distinct prognostic roles in the microenvironment of CRC [54]. However, the regulatory relationship between pyroptosis and macrophage polarization in CRC requires further investigation.

To further unravel the diverse molecular mechanisms underlying the prognostic differences attributed to the CRC primary tumor location, this study identified five prognostic signatures, *CHMP7*, *CXCL13*, *NLRP7*, *TDGF1*, and *TP63*, among 134 pyroptosis-related DEGs. Among these, patients with high expression of *CHMP7*, *CXCL13*, *NLRP7*, and *TDGF1* had a significantly favorable prognosis, whereas increased expression of *TP63* correlated with an adverse prognosis. Experimental data also confirmed that *TP63* was

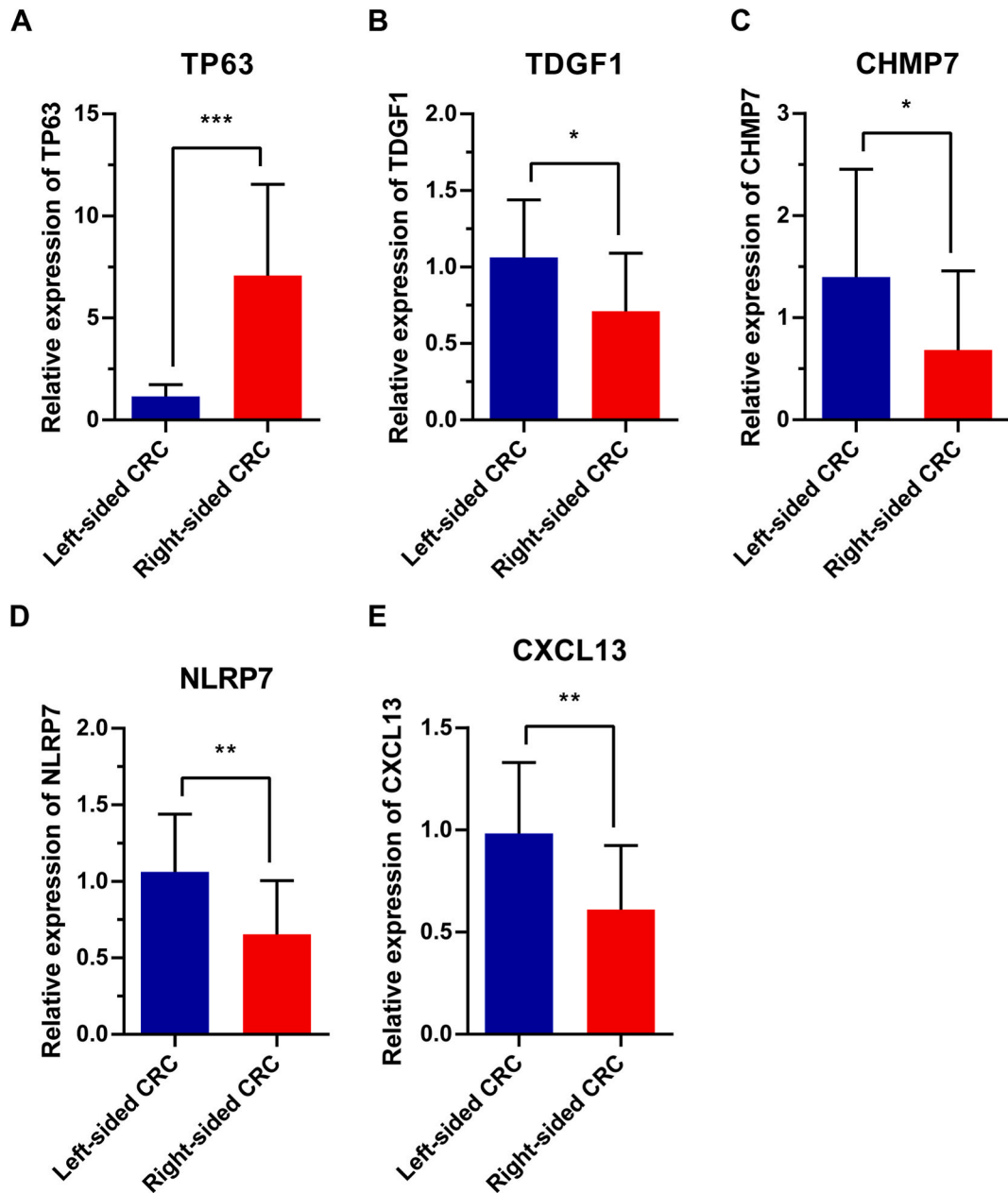


Fig. 8. Expression validation of *five* prognostic signatures including *TP63* (A), *TDGF1* (B), *CHMP7* (C), *NLRP7* (D), and *CXCL13* (E) using RT-qPCR. \* $p < 0.05$ , \*\* $p < 0.01$ , \*\*\* $p < 0.001$ . RT-qPCR, reverse transcription-quantitative PCR.

significantly overexpressed in right-sided CRC with a worse prognosis, whereas the remaining four genes were significantly overexpressed in left-sided CRC with a better prognosis. Therefore, aberrant expression of these genes in primary tumors could be predictors of prognosis in patients with CRC.

It has been suggested that *TDGF1* expression can predict the prognosis of colorectal adenocarcinoma [55], which is consistent with our findings. *TDGF1* also serves as a predictive marker of metachronous metastasis in CRC [56]. *TP63* is associated with pyroptosis and autophagy and can be used to predict the possibility of early recurrence in patients with stage I–III CRC [57]. Autophagy and pyroptosis, the main types of programmed cell necrosis, may jointly determine the fate of malignant cells [58]. Therefore, as a prognostic risk factor for CRC, *TP63* may participate in the process of pyroptosis and autophagy at the early stage of the tumor and further triggers tumor progression. *CXCL13* plays an important role in metastasis and recurrence of advanced CRC [59], and its expression level is related to disease-free survival and OS of patients with CRC [60], which was further confirmed in the current study. *CXCL13* was also found to be substantially associated with tumor immune invasion by CD8<sup>+</sup> T cells [61]. CD8<sup>+</sup> T cell infiltration was found to differ considerably between left- and right-sided CRC; therefore, we hypothesized that the prognostic regulatory mechanism

of *CXCL13* may be related to the infiltration level of CD8<sup>+</sup> T cells. However, the pyroptosis regulatory mechanisms of these genes have rarely been reported; hence, additional experiments are necessary to confirm these hypotheses.

In terms of the pyroptosis regulator *NLRP7*, our results suggested that *NLRP7* may play a prognostic protective role in CRC. NLR containing *NLRP7* was found to assemble and activate the inflammasome complex, including caspase-1, to promote the expression of tumor necrosis factor- $\alpha$  and interleukin-1 $\beta$  and induce pyroptosis [62–64]. This regulatory mechanism can be observed in human macrophages [65], and the macrophage infiltration is believed to differ markedly between left- and right-sided CRC and affect the tumor microenvironment of CRC. *NLRP7* reportedly induces the polarization of CRC tumor-associated macrophages and affects tumor progression through USP10 deubiquitination [66]. Based on these findings, we speculate that *NLRP7* can promote inflammasome formation and induce pyroptosis in the left-sided CRC, which suppresses tumor recurrence and metastasis by modulating macrophage polarization to activate the immune response.

Nevertheless, the limitations of this study need to be addressed. Although we collected clinical samples to perform the experiments, the small sample size and lack of prognostic information restricted the further validation of relationships between candidate gene expression and clinical characteristics of patients. Therefore, subsequent experimental studies based on a large sample size are needed to investigate the relationships between age, sex, and tumor stage and the expression of the five candidate genes, as well as their impacts on the prognosis of left- and right-sided CRC. More importantly, the findings of the present study can guide future investigations, affording a basis for *in vivo* and *in vitro* experiments to investigate the pyroptosis regulatory mechanism of the five prognostic signatures in CRC and the molecular mechanisms involved in macrophage polarization.

## 5. Conclusions

In summary, left- and right-sided CRC differed substantially in survival status, clinical characteristics, immune infiltration, and somatic mutations. To uncover the underlying molecular mechanism of pyroptosis, five pyroptosis-related gene signatures, which served as potential biomarkers, were identified to stratify and predict CRC prognostic by constructing a prognostic model. These findings may help predict and improve clinical outcomes in patients with CRC with different tumor locations.

## Funding

The authors received no specific funding for this work.

## Data availability

The data used to support the findings of this study are included within the article.

## CRedit authorship contribution statement

**Shibi Luo:** Writing – original draft, Conceptualization. **Shenggang Cai:** Writing – original draft. **Rong Zhao:** Data curation. **Lin Xu:** Project administration. **Xiaolong Zhang:** Methodology. **Xiaolei Gong:** Investigation. **Zhiping Zhang:** Visualization, Supervision. **Qiyu Liu:** Writing – review & editing, Conceptualization.

## Declaration of competing interest

The authors declare that they have no known competing financial interests or personal relationships that could have appeared to influence the work reported in this paper.

## Acknowledgement

None.

## Abbreviations

CRC	colorectal cancer
TCGA	The Cancer Genome Atlas
GEO	Gene Expression Omnibus
OS	overall survival
DEG	differentially expressed gene
FC	fold change
GSEA	gene set enrichment analysis
GO-BP	gene ontology biological processes
KEGG	Kyoto Encyclopedia of Genes and Genomes
NES	normalized enrichment score
RT-qPCR	reverse transcription-quantitative polymerase chain reaction

## Appendix A. Supplementary data

Supplementary data to this article can be found online at <https://doi.org/10.1016/j.heliyon.2024.e28091>.

## References

- [1] L. Liang, et al., Distinguishable prognostic signatures of left- and right-sided colon cancer: a study based on sequencing data, *Cell. Physiol. Biochem.* 48 (2) (2018) 475–490.
- [2] L. Liu, et al., Comprehensive analysis of pyroptosis-related long noncoding RNA immune infiltration and prediction of prognosis in patients with colon cancer, *JAMA Oncol.* 2022 (2022) 2035808.
- [3] G. Brandi, et al., Is post-transplant chemotherapy feasible in liver transplantation for colorectal cancer liver metastases? *Cancer Commun.* 40 (9) (2020) 461–464.
- [4] M. Santoni, et al., The impact of gender on the efficacy of immune checkpoint inhibitors in cancer patients: the MOUSEION-01 study, *Crit. Rev. Oncol. Hematol.* 170 (2022) 103596.
- [5] M. Santoni, et al., Complete remissions following immunotherapy or immuno-oncology combinations in cancer patients: the MOUSEION-03 meta-analysis, *Cancer Immunol. Immunother.* 72 (6) (2023) 1365–1379.
- [6] A. Rizzo, et al., Dose reduction and discontinuation of standard-dose regorafenib associated with adverse drug events in cancer patients: a systematic review and meta-analysis, *Ther. Adv. Med. Oncol.* 12 (2020) 1758835920936932.
- [7] L.H. Biller, D. Schrag, Diagnosis and treatment of metastatic colorectal cancer: a review, *JAMA* 325 (7) (2021) 669–685.
- [8] K. Helvacı, et al., Comparison of clinicopathological and survival features of right and left colon cancers, *J. Buon* 24 (5) (2019) 1845–1851.
- [9] R. Imperial, et al., Comparative proteogenomic analysis of right-sided colon cancer, left-sided colon cancer and rectal cancer reveals distinct mutational profiles, *Mol. Cancer* 17 (1) (2018) 177.
- [10] K. Mukund, et al., Right and left-sided colon cancers - specificity of molecular mechanisms in tumorigenesis and progression, *BMC Cancer* 20 (1) (2020) 317.
- [11] Y. Jiang, et al., Discovering the molecular differences between right- and left-sided colon cancer using machine learning methods, *BMC Cancer* 20 (1) (2020) 1012.
- [12] K. Kim, et al., Differences in clinical features and oncologic outcomes between metastatic right and left colon cancer, *J. Buon* 23 (7) (2018) 11–18.
- [13] J.W. Holch, et al., The relevance of primary tumour location in patients with metastatic colorectal cancer: a meta-analysis of first-line clinical trials, *Eur. J. Cancer* 70 (2017) 87–98.
- [14] S. Stintzing, et al., Understanding the role of primary tumour localisation in colorectal cancer treatment and outcomes, *Eur. J. Cancer* 84 (2017) 69–80.
- [15] M. Yahagi, et al., The worse prognosis of right-sided compared with left-sided colon cancers: a systematic review and meta-analysis, *J. Gastrointest. Surg.* 20 (3) (2016) 648–655.
- [16] J. Ruan, S. Wang, J. Wang, Mechanism and regulation of pyroptosis-mediated in cancer cell death, *Chem. Biol. Interact.* 323 (2020) 109052.
- [17] Y. Fang, et al., Pyroptosis: a new frontier in cancer, *Biomed. Pharmacother.* 121 (2020) 109595.
- [18] R. Loveless, R. Bloomquist, Y. Teng, Pyroptosis at the forefront of anticancer immunity, *J. Exp. Clin. Cancer Res.* 40 (1) (2021) 264.
- [19] Z. Zhuang, et al., Development and validation of a robust pyroptosis-related signature for predicting prognosis and immune status in patients with colon cancer, *JAMA Oncol.* 2021 (2021) 5818512.
- [20] B. Luo, et al., Identification of the pyroptosis-related gene signature and risk score model for colon adenocarcinoma, *Front. Genet.* 12 (2021) 771847.
- [21] C.B. Zhou, J.Y. Fang, The role of pyroptosis in gastrointestinal cancer and immune responses to intestinal microbial infection, *Biochim. Biophys. Acta Rev. Canc.* 1872 (1) (2019) 1–10.
- [22] G. Tan, et al., HMGB1 released from GSDME-mediated pyroptotic epithelial cells participates in the tumorigenesis of colitis-associated colorectal cancer through the ERK1/2 pathway, *J. Hematol. Oncol.* 13 (1) (2020) 149.
- [23] R. Jiang, et al., MiR-21-5p induces pyroptosis in colorectal cancer via TGFBI, *Front. Oncol.* 10 (2020) 610545.
- [24] F. Su, et al., Long non-coding RNA nuclear paraspeckle assembly transcript 1 regulates ionizing radiation-induced pyroptosis via microRNA-448/gasdermin E in colorectal cancer cells, *Int. J. Oncol.* 59 (4) (2021).
- [25] K.R. Rosenbloom, et al., The UCSC Genome Browser database: 2015 update, *Nucleic Acids Res.* 43 (2015) D670–D681 (Database issue).
- [26] J. Harrow, et al., GENCODE: the reference human genome annotation for the ENCODE Project, *Genome Res.* 22 (9) (2012) 1760–1774.
- [27] I. Patil, Visualizations with statistical details: the 'ggstatsplot' approach, *J. Open Source Softw.* 6 (61) (2021) 3167.
- [28] T. Therneau, T. Therneau, P. Grambsch, *Modeling Survival Data: Extending the Cox Model* (Statistics for Biology and Health), 2000.
- [29] A.M. Newman, et al., Robust enumeration of cell subsets from tissue expression profiles, *Nat. Methods* 12 (5) (2015) 453–457.
- [30] A. Mayakonda, et al., Maftools: efficient and comprehensive analysis of somatic variants in cancer, *Genome Res.* 28 (11) (2018) 1747–1756.
- [31] G.K. Smyth, Limma: linear models for microarray data, in: *Bioinformatics and Computational Biology Solutions Using R and Bioconductor*, 2013.
- [32] R.A.M. Villanueva, Z.J. Chen, *ggplot2: Elegant Graphics for Data Analysis*, Taylor & Francis, 2019.
- [33] W. Song, et al., Identification of pyroptosis-related subtypes, the development of a prognosis model, and characterization of tumor microenvironment infiltration in colorectal cancer, *Oncol. Immunology* 10 (1) (2021) 1987636.
- [34] Y. Ye, Q. Dai, H. Qi, A novel defined pyroptosis-related gene signature for predicting the prognosis of ovarian cancer, *Cell Death Dis.* 7 (1) (2021) 71.
- [35] M. Zhang, et al., A risk score system based on DNA methylation levels and a nomogram survival model for lung squamous cell carcinoma, *Int. J. Mol. Med.* 46 (1) (2020) 252–264.
- [36] G. Yu, et al., clusterProfiler: an R package for comparing biological themes among gene clusters, *OMICS* 16 (5) (2012) 284–287.
- [37] A. Liberzon, et al., The Molecular Signatures Database (MSigDB) hallmark gene set collection, *Cell Syst* 1 (6) (2015) 417–425.
- [38] C.T. Yeh, G.Y. Liao, T. Emura, Sensitivity analysis for survival prognostic prediction with gene selection: a copula method for dependent censoring, *Biomedicines* 11 (3) (2023).
- [39] J.P. Klein, M.L. Moeschberger, *Survival Analysis: Techniques for Censored and Truncated Data*, Springer, New York, 2003.
- [40] Z. Zhang, et al., Nomogram for survival analysis in the presence of competing risks, *Ann. Transl. Med.* 5 (20) (2017) 403.
- [41] M. Kanehisa, S. Goto, KEGG: kyoto encyclopedia of genes and genomes, *Nucleic Acids Res.* 28 (1) (2000) 27–30.
- [42] T.G.O. Consortium, The gene ontology resource: 20 years and still going strong, *Nucleic Acids Res.* 47 (D1) (2019) D330–d338.
- [43] S.Y. Yang, M.S. Cho, N.K. Kim, Difference between right-sided and left-sided colorectal cancers: from embryology to molecular subtype, *Expert Rev. Anticancer Ther.* 18 (4) (2018) 351–358.
- [44] D.J. Kerr, E. Domingo, R. Kerr, Is sidedness prognostically important across all stages of colorectal cancer? *Lancet Oncol.* 17 (11) (2016) 1480–1482.
- [45] D. Shida, et al., Prognostic impact of primary tumor location in Stage III colorectal cancer-right-sided colon versus left-sided colon versus rectum: a nationwide multicenter retrospective study, *J. Gastroenterol.* 55 (10) (2020) 958–968.
- [46] C.E. Degro, et al., Survival rates and prognostic factors in right- and left-sided colon cancer stage I-IV: an unselected retrospective single-center trial, *Int. J. Colorectal Dis.* 36 (12) (2021) 2683–2696.
- [47] M.Z. Qiu, et al., Comparison of survival between right-sided and left-sided colon cancer in different situations, *Cancer Med.* 7 (4) (2018) 1141–1150.
- [48] L. Mangone, et al., Colon cancer survival differs from right side to left side and lymph node harvest number matter, *BMC Publ. Health* 21 (1) (2021) 906.

- [49] H. Shen, et al., Different treatment strategies and molecular features between right-sided and left-sided colon cancers, *World J. Gastroenterol.* 21 (21) (2015) 6470–6478.
- [50] R. Warschkow, et al., Better survival in right-sided versus left-sided stage I - III colon cancer patients, *BMC Cancer* 16 (2016) 554.
- [51] D. Frank, J.E. Vince, Pyroptosis versus necroptosis: similarities, differences, and crosstalk, *Cell Death Differ.* 26 (1) (2019) 99–114.
- [52] S.W. Sun, et al., Pyroptotic cell-derived microparticle: an atherogenic factor in infectious diseases, *Med. Hypotheses* 146 (2021) 110370.
- [53] K.A. Deets, et al., Inflammasome activation leads to cDC1-independent cross-priming of CD8 T cells by epithelial cell-derived antigen, *Elife* 10 (2021).
- [54] J.P. Väyrynen, et al., The prognostic role of macrophage polarization in the colorectal cancer microenvironment, *Cancer Immunol. Res.* 9 (1) (2021) 8–19.
- [55] Y.L. Sun, et al., A prognostic model based on the immune-related genes in colon adenocarcinoma, *Int. J. Med. Sci.* 17 (13) (2020) 1879–1896.
- [56] N. Miyoshi, et al., TDGF1 is a novel predictive marker for metachronous metastasis of colorectal cancer, *Int. J. Oncol.* 36 (3) (2010) 563–568.
- [57] S. Mo, et al., Prognostic and predictive value of an autophagy-related signature for early relapse in stages I-III colon cancer, *Carcinogenesis* 40 (7) (2019) 861–870.
- [58] Z. Zheng, G. Li, Mechanisms and therapeutic regulation of pyroptosis in inflammatory diseases and cancer, *Int. J. Mol. Sci.* 21 (4) (2020).
- [59] X.W. Qi, et al., Expression features of CXCR5 and its ligand, CXCL13 associated with poor prognosis of advanced colorectal cancer, *Eur. Rev. Med. Pharmacol. Sci.* 18 (13) (2014) 1916–1924.
- [60] X. Li, et al., The prognostic value of CXC subfamily ligands in stage I-III patients with colorectal cancer, *PLoS One* 14 (4) (2019) e0214611.
- [61] J. Liu, et al., Identification and development of a novel invasion-related gene signature for prognosis prediction in colon adenocarcinoma, *Cancer Cell Int.* 21 (1) (2021) 101.
- [62] Y. Zhou, et al., Virulent *Mycobacterium bovis* Beijing strain activates the NLRP7 inflammasome in THP-1 macrophages, *PLoS One* 11 (4) (2016) e0152853.
- [63] J. Carriere, A. Dorfleutner, C. Stehlik, NLRP7: from inflammasome regulation to human disease, *Immunology* 163 (4) (2021) 363–376.
- [64] A.D. Radian, et al., ATP binding by NLRP7 is required for inflammasome activation in response to bacterial lipopeptides, *Mol. Immunol.* 67 (2 Pt B) (2015) 294–302.
- [65] S. Khare, et al., An NLRP7-containing inflammasome mediates recognition of microbial lipopeptides in human macrophages, *Immunity* 36 (3) (2012) 464–476.
- [66] B. Li, et al., NLRP7 deubiquitination by USP10 promotes tumor progression and tumor-associated macrophage polarization in colorectal cancer, *J. Exp. Clin. Cancer Res.* 40 (1) (2021) 126.